Structural Engineering and Mechanics, *Vol. 62, No. 2 (2017) 151-162*
DOI: https://doi.org/10.12989/sem.2017.62.2.151

Assessments of dissipative structure-dependent integration methods

Shuenn-Yih Chang*

Department of Civil Engineering, National Taipei University of Technology,
1, Section 3, Jungshiau East Road, Taipei 106-08, Republic of China

(Received October 19, 2016, Revised December 20, 2016, Accepted December 24, 2016)

Abstract. Two Chang-α dissipative family methods and two KR-α family methods were developed for time integration recently. Although the four family methods are in the category of the dissipative structure-dependent integration methods, their performances may be drastically different due to the detrimental property of weak instability or overshoot for the two KR-α family methods. This weak instability or overshoot will result in an adverse overshooting behavior or even numerical instability. In general, the four family methods can possess very similar numerical properties, such as unconditional stability, second-order accuracy, explicit formulation and controllable numerical damping. However, the two KR-α family methods are found to possess a weak instability property or overshoot in the high frequency responses to any nonzero initial conditions and thus this property will hinder them from practical applications. Whereas, the two Chang-α dissipative family methods have no such an adverse property. As a result, the performances of the two Chang-α dissipative family methods are much better than for the two KR-α family methods. Analytical assessments of all the four family methods are conducted in this work and numerical examples are used to confirm the analytical predictions.

Keywords: weak instability; nonzero initial conditions; overshoot; structure-dependent integration method

1. Introduction

Some structure-dependent integration methods have been developed for time integration since they can simultaneously integrate unconditional stability and explicit formulation together (Chang 2002, 2007a, 2009, 2010, 2014a, Chen and Ricles 2008, Gui *et al*. 2014). The most significant difference between this type of integration methods and the traditional integration methods (Newmark 1959, Bathe and Wilson 1978, Hilber *et al*. 1977, Fung 2001, 2002, Civalek 2006, 2007, 2013, Gao, *et al*. 2012, Hadianfard 2012, Alamatian 2013) is the coefficients of the difference equation for displacement and/or velocity increment. In general, these coefficients are scalar constants for conventional integration methods while for structure-dependent integration methods they can be functions of the initial structural properties and step size. It is promising for structure-dependent integration methods to have an explicit formulation and unconditional stability together since this combination enables this type of the integration methods to be computationally efficient. An explicit formulation will involve no nonlinear iterations for each time step for a nonlinear system. Notice that an iteration procedure is generally very time consuming for each iteration and thus it costs many computational efforts for a traditional implicit integration method. Meanwhile, the unconditional stability might allow the choice of a relatively large time step for conducting step-by-step integration based on accuracy consideration only.

The above-mentioned structure-dependent integration methods have no numerical damping. A favorable numerical damping can effectively suppress or even filter out the spurious growth of the high frequency modes while the low frequency responses can be very accurately integrated. Thus, it is preferable for an integration method to possess such a dissipative property (Hilber *et al*. 1977, Wood *et al*. 1981, Chung and Hulbert 1993, Krenk 2008, Bathe and Noh 2012). For this purpose, some families of the structure-dependent integration methods have been developed to have this desired numerical damping recently (Chang 2014b, c, 2015a, Chang *et al*. 2015, Kolay and Ricles 2014, 2016). These family methods can have favorable numerical properties, such as unconditional stability, explicit formulation, second-order accuracy and numerical damping. However, some adverse properties are also found for the specific family methods, such as the weak instability and overshoot for nonzero initial conditions for the two KR-α family methods, a poor capability to capture structural nonlinearity for one of the KR-α family method, and the unusual overshoot in the high frequency forced vibration responses for both the two KR-α family methods and the two Chang-α dissipative family methods. As a result, it is of great interest to evaluate their actual performances in the step-by-step integration. For this purpose, the four family methods are chosen for this study. In this work, the basic numerical properties of the four family methods for linear elastic systems are summarized and compared first. In addition, the adverse properties are also thoroughly explored subsequently.

*Corresponding author, Professor
E-mail: changsy@ntut.edu.tw

ISSN: 1225-4568 (Print), 1598-6217 (Online)

2. General formulation

The first Chang-α dissipative family method (CDM1) (Chang 2014c) has the same asymptotic form of the equation of motion and the difference equation for velocity increment as those of the HHT-α method. However, its difference equation for displacement increment is significantly different from that of the HHT-α method. In general, the general formulation of the first Chang-α dissipative family method can be expressed as

$$\begin{aligned} & ma_{i+1}+cv_{i+1}+(1+\alpha)kd_{i+1}-\alpha kd_i=(1+\alpha)f_{i+1}-\alpha f_i \\ & d_{i+1}=(1-\beta_1)d_{i-1}+\beta_1 d_i+\beta_2(\Delta t)v_i+\beta_3(\Delta t)^2 a_i \\ & v_{i+1}=v_i+(\Delta t)\left[(1-\gamma)a_i+\gamma a_{i+1}\right] \end{aligned} \tag{1}$$

On the other hand, the second Chang-α dissipative family method (CDM2) (Chang 2015a) inherits both the asymptotic form of the equation of motion and difference equation for velocity increment from the WBZ-α method although its difference equation for displacement increment is different from that of the WBZ-α method. The general formulation of CDM2 can be written as

$$\begin{aligned} & (1-\alpha)ma_{i+1}+\alpha ma_i+cv_{i+1}+kd_{i+1}=f_{i+1} \\ & d_{i+1}=d_i+\beta_1(\Delta t)v_i+\beta_2(\Delta t)^2 a_i+\beta_3(\Delta t)^2 a_{i-1} \\ & v_{i+1}=v_i+(\Delta t)\left[(1-\gamma)a_i+\gamma a_{i+1}\right] \end{aligned} \tag{2}$$

where d_i, v_i, a_i and f_i are introduced to represent the approximate nodal displacement, velocity, acceleration and external force at the i-th time step, respectively. It is found from the second line of Eq. (1) that the determination of d_{i+1} will involve the two previously step data and thus CDM1 is a two-step method. Similarly, CDM2 is also a two-step method. Consequently, a distinct starting procedure is generally needed for both CDM1 and CDM2. The structure-dependent coefficients β_1, β_2 and β_3 for CDM1 and CDM2 are found to be

$$\begin{cases} \beta_1=1+\dfrac{1}{D_1}\alpha\beta\sigma\Omega_0^2 \\ \beta_2=\dfrac{1}{D_1}(1+2\gamma\xi\Omega_0) \\ \beta_3=\dfrac{1}{D_1}\left[\frac{1}{2}-(\beta-\frac{1}{2}\gamma)2\xi\Omega_0\right] \end{cases} \text{CDM1}$$

$$\begin{cases} \beta_1=\dfrac{1}{D_2}(1-\alpha+2\gamma\xi\Omega_0) \\ \beta_2=\dfrac{1}{D_2}\left[\frac{1}{2}-\frac{1}{2}\alpha-\alpha\beta-(\beta-\frac{1}{2}\gamma)2\xi\Omega_0\right] \\ \beta_3=\dfrac{1}{D_2}(\alpha\beta) \end{cases} \text{CDM2} \tag{3}$$

where $\Omega_0=\omega_0(\Delta t)$ and $\omega_0=\sqrt{k_0/m}$ is an initial natural frequency, where k_0 is an initial stiffness. In addition, $D_1=1+2\gamma\xi\Omega_0+(1+\alpha)\beta\sigma\Omega_0^2$, $D_2=1-\alpha+2\gamma\xi\Omega_0+\beta\sigma\Omega_0^2$, and ξ is a viscous damping ratio; α, β and γ are the parameters to govern the numerical properties. Notice that σ is a stability amplification factor, which can be applied to enlarge the unconditional stability range for a general structure-dependent integration method (Chang 2015b). In order to have desired numerical properties, such as explicit formulation, unconditional stability and numerical damping, the following relationships are recommended for CDM1 and CDM2

$$\begin{aligned} & -\tfrac{1}{3}\le\alpha\le 0,\ \ \beta=\tfrac{1}{4}(1-\alpha)^2,\ \ \gamma=\tfrac{1}{2}-\alpha \ \text{CDM1} \\ & -1\le\alpha\le 0,\ \ \beta=\tfrac{1}{4}(1-\alpha)^2,\ \ \gamma=\tfrac{1}{2}-\alpha \ \text{CDM2} \end{aligned} \tag{4}$$

Since the spectral radius ρ_∞ in the limit $\Omega_0\to\infty$ can be considered as an indicator for numerical dissipation, it is of interest to construct the correlations between α and ρ_∞ for both CDM1 and CDM2. As a result, they are found to be

$$\begin{aligned} & \alpha=\frac{\rho_\infty-1}{\rho_\infty+1},\ \ \tfrac{1}{2}\le\rho_\infty\le 1 \ \text{CDM1} \\ & \alpha=\frac{\rho_\infty-1}{\rho_\infty+1},\ \ 0\le\rho_\infty\le 1 \ \text{CDM2} \end{aligned} \tag{5}$$

The variation of α from −1/3 to 0 corresponds to the variation of ρ_∞ from 1/2 to 1 for CDM1. Similarly, the variation of α from −1 to 0 corresponds to the variation of ρ_∞ from 0 to 1 for CDM2. It is evident that both CDM1 and CDM2 can have controllable numerical dissipation. Notice that a zero-damping ratio can be generally achieved for both the two dissipative family methods.

On the other hand, the general formulation of the first KR-α method (KRM1) (Kolay and Ricles 2014) for a single degree of freedom system can be written as

$$\begin{aligned} & (1-\alpha_3)ma_{i+1}+\alpha_3 ma_i+(1-\alpha_f)cv_{i+1}+\alpha_f cv_i+ \\ & (1-\alpha_f)k_{i+1}d_{i+1}+\alpha_f k_i d_i=(1-\alpha_f)f_{i+1}+\alpha_f f_i \\ & d_{i+1}=d_i+(\Delta t)v_i+\alpha_2(\Delta t)^2 a_i \\ & v_{i+1}=v_i+\alpha_1(\Delta t)a_i \end{aligned} \tag{6}$$

and that for the second KR-α method (KRM2) (Kolay and Ricles 2016) is found to be

$$\begin{aligned} & (1-\alpha_3)ma_{i+1}+\alpha_3 ma_i+(1-\alpha_f)cv_{i+1}+\alpha_f cv_i+ \\ & (1-\alpha_f)kd_{i+1}+\alpha_f kd_i=(1-\alpha_f)f_{i+1}+\alpha_f f_i \\ & d_{i+1}=d_i+\alpha_1(\Delta t)v_i+\alpha_2(\Delta t)^2 a_i \\ & v_{i+1}=v_i+(\Delta t)\left[(1-\gamma)a_i+\gamma a_{i+1}\right] \end{aligned} \tag{7}$$

where the structure-dependent coefficients α_1, α_2 and α_3 for KRM1 and KRM2 are found to be

$$\begin{cases} \alpha_1=\dfrac{1}{D_3},\ \alpha_2=\dfrac{1}{D_3}(\frac{1}{2}+\gamma) \\ \alpha_3=\dfrac{1}{D_3}(\alpha_m+\alpha_m 2\gamma\xi\Omega_0+\alpha_f\beta\sigma\Omega_0^2) \end{cases} \text{KRM1}$$

$$\begin{cases} \alpha_1=\dfrac{1}{D_3}(1+\gamma 2\xi\Omega_0),\ \alpha_2=\dfrac{1}{D_3}\left[\frac{1}{2}-(\beta-\frac{1}{2}\gamma)2\xi\Omega_0\right] \\ \alpha_3=\dfrac{1}{D_3}(\alpha_m+\alpha_m 2\gamma\xi\Omega_0+\alpha_f\beta\sigma\Omega_0^2) \end{cases} \text{KRM2} \tag{8}$$

where $D_3 = 1 + 2\gamma\xi\Omega_0 + \beta\sigma\Omega_0^2$; and scalar coefficients α_m, α_f, β and γ are found to be

$$\alpha_m = \frac{2\rho_\infty - 1}{\rho_\infty + 1}, \quad \alpha_f = \frac{\rho_\infty}{\rho_\infty + 1}$$
$$\beta = \frac{1}{4}\left(1 - \alpha_m + \alpha_f\right)^2, \quad \gamma = \frac{1}{2} - \alpha_m + \alpha_f \tag{9}$$

In Eq. (6), both the difference equation for displacement and that for velocity increment are structure dependent for KRM1. Whereas, for KRM2, only the difference equation for displacement increment is structure dependent. This is the major difference between KRM1 and KRM2 in formulations. Apparently, the free parameter ρ_∞ can be applied to control the numerical properties of KRM1 and KRM2 and it varies in the range of $0 \le \rho_\infty \le 1$. The case of ρ_∞=1 implies zero damping while ρ_∞=0 has the largest numerical damping.

3. Numerical properties of linear elastic systems

Since the basic analysis of each family method has been conducted before, thus, it will not be performed herein again. However, the basic numerical properties are summarized for comparison, such as stability, period distortion, numerical dissipation and overshoot. The cases of ρ_∞=1 and $\frac{1}{2}$ will be generally considered. Fig. 1 shows the variation of relative period error with $\Delta t/T_0$ for the four family methods. The curves for the four family methods are overlapped together for ρ_∞=1. Whereas, for $\rho_\infty = \frac{1}{2}$, only CDM1, KRM1 and KRM2 are coincided together. Apparently, CDM2 exhibits a larger period distortion for a given $\Delta t/T_0$ when compared to the other three family methods. The variation of the numerical damping ratio with $\Delta t/T_0$ for each family method is plotted in Fig. 2.

It is seen that the four family methods have no numerical dissipation for ρ_∞=1 while for $\rho_\infty = \frac{1}{2}$ CDM2 has larger numerical damping when compared to the other three family methods, whose curves are overlapped together. This figure confirm that the four family methods can have desired numerical damping. Variations of spectral radii with $\Delta t/T_0$ for the four family methods are plotted in Fig. 3. It is found that the spectral radius is always equal to 1 for any value of $\Delta t/T_0$ for the four family methods for ρ_∞=1. Whereas, for $\rho_\infty = \frac{1}{2}$, the spectral radius is equal to 1 for a small value of $\Delta t/T_0$ and subsequently it decreases gradually with the increase of $\Delta t/T_0$. Finally, it will become an asymptotic constant and is equal to ρ_∞ as $\Delta t/T_0$ is greater than a certain value. Notice that the curves for CDM1, KRM1 and KRM2 are coincided together for $\rho_\infty = \frac{1}{2}$.

An adverse overshooting property in the free vibration

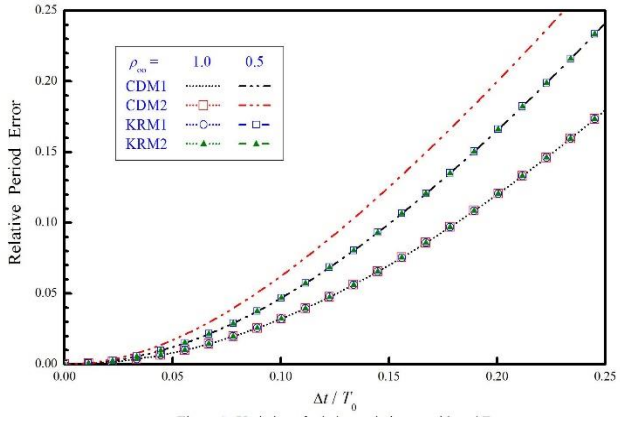

Fig. 1 Variation of relative period error with $\Delta t/T_0$

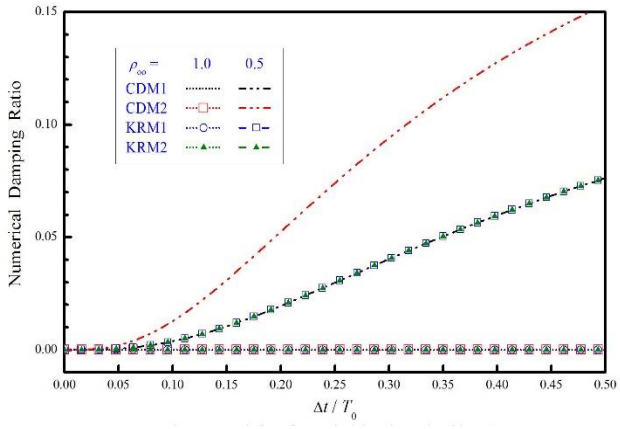

Fig. 2 Variation of numerical damping ratio with $\Delta t/T_0$

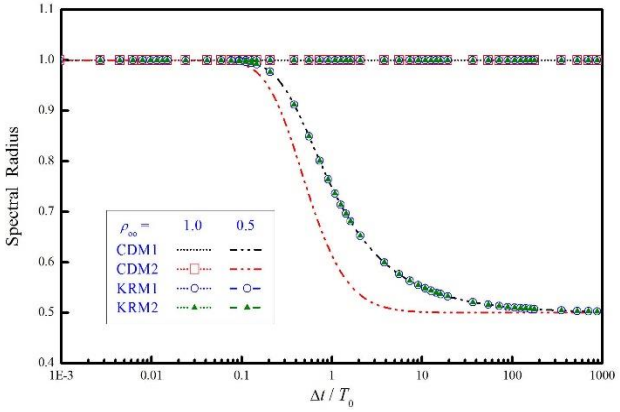

Fig. 3 Variation of spectral radius with $\Delta t/T_0$

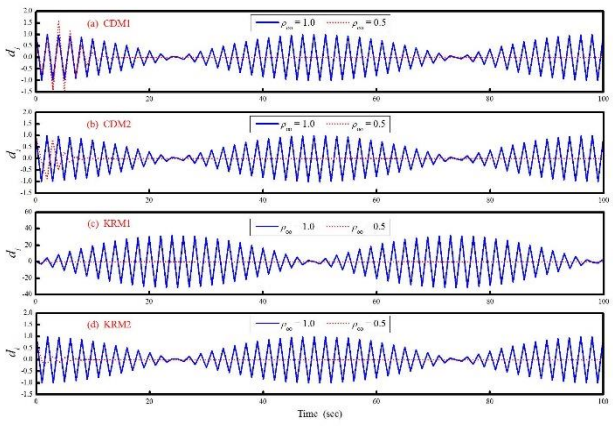

Fig. 4 Comparison of overshoot response in displacement

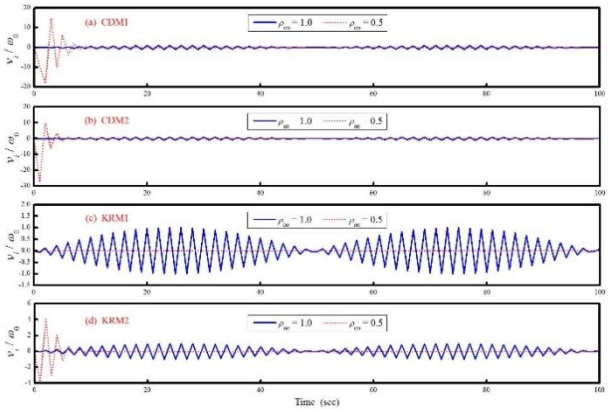

Fig. 5 Comparison of overshoot response in velocity

responses of the high frequency modes has been found in the Wilson-θ method by Goudreau and Taylor in 1972. Later, a technique to detect such an unusual overshoot behavior has been further proposed by Hilber and Hughes in 1978. The tendency of an integration method to overshoot the exact solution can be evaluated by calculating the free vibration response of a linear elastic, single degree of freedom system for the current time step based on the previous step data as $\Omega_0\to\infty$. As a result, the results for CDM1, CDM2, KRM1 and KRM2 for the limiting cases of $\Omega_0\to\infty$ are found to be

$$\begin{cases} d_{i+1} \approx \left[1-\dfrac{\frac{1}{2}}{(1+\alpha)\beta}\right] d_i \\ v_{i+1} \approx \left(\dfrac{\frac{1}{2}\gamma}{\beta}-1\right)\Omega_0\omega_0 d_i + \left(1-\dfrac{\gamma}{\beta}\right) v_i \end{cases} \text{CDM1}$$

$$\begin{cases} d_{i+1} \approx \left[1-\dfrac{2}{(1-\alpha)}\right] d_i \\ v_{i+1} \approx \left(\dfrac{\frac{1}{2}\gamma}{\beta}-1\right)\Omega_0\omega_0 d_i + \left(1-\dfrac{\gamma}{\beta}\right) v_i \end{cases} \text{CDM2}$$

$$\begin{cases} d_{i+1} \approx \left(1-\dfrac{\gamma+\frac{1}{2}}{\beta}\right) d_i + (\Delta t) v_i \\ v_{i+1} \approx -\dfrac{1}{\beta}\left(\dfrac{d_i}{\Delta t}\right) + v_i \end{cases} \text{KRM1} \qquad (10)$$

$$\begin{cases} d_{i+1} \approx \left(1-\dfrac{\frac{1}{2}}{\beta}\right) d_i \\ v_{i+1} \approx \left(\dfrac{\frac{1}{2}\gamma}{\beta}-1\right)\Omega_0\omega_0 d_i + \left(1-\dfrac{\gamma}{\beta}\right) v_i \end{cases} \text{KRM2}$$

This equation reveals that there is no overshoot behavior in displacement for any member of each family method while it generally has a tendency to overshoot linearly in Ω_0 in the velocity equation due to the initial displacement term for CDM1, CDM2 and KRM2. Notice that KRM1 exhibits no overshoot in velocity.

In order to confirm the overshooting behaviors of the four family methods, the displacement and velocity responses are calculated by using the four family methods with ρ_∞=1 and $\frac{1}{2}$. The initial conditions of d_0=1 and v_0=0 are taken. The time step of $\Delta t=10T_0$ is adopted for each family method. The velocity term is normalized by the initial natural frequency of the system in order to have the same unit as displacement. Calculated results are shown in Figs. 4 and 5. It is seen in Fig. 4 that CDM1, CDM2 and KRM2 generally show no overshoot in the displacement responses and these results are consistent with the analytical results. Whereas, an overshoot is found in the displacement response for KRM1 and this result is inconsistent with the analytical prediction. The cause of this overshoot will be further explored later. On the other hand, in Fig. 5, KRM1 shows no overshoot both for ρ_∞=1 and 0.5. Whereas, an overshooting behavior is found in the velocity response of CDM1, CDM2 and KRM2 for $\rho_\infty=\frac{1}{2}$ although there is no overshoot in the velocity response of CDM1, CDM2 and KRM2 for ρ_∞=1. It is found that for ρ_∞=1 one can have $\gamma/(2\beta)-1=0$ for the four family methods. Hence, the linearly proportional term in Ω_0 in the velocity equation as shown in Eq. (10) will disappear for CDM1, CDM2 and KRM2. As a result, the overshoot behaviors in velocity is generally consistent with the analytical predictions.

4. Numerical properties of nonlinear systems

In the previous section, the numerical properties of the four family methods are summarized and compared. However, it is still very important to investigate their performances to solve nonlinear systems. A parameter named the instantaneous degree of nonlinearity has been introduced by Chang (2017b) to monitor the stiffness change for a nonlinear system. It is defined as the ratio of the stiffness at the end of the i-th time step over the initial stiffness and is $\delta_i=k_i/k_0$. Thus, it is implied by δ_i=1 that the instantaneous stiffness at the end of the i-th time step is equal to the initial stiffness. Whereas, δ_i>1 means stiffness hardening and the instantaneous stiffness larger than the initial stiffness at the end of the i-th time step; and $0<\delta_i<1$ means stiffness softening and the instantaneous stiffness less than the initial stiffness.

A structure-dependent integration method can have unconditional stability for $\delta_i\le 1$ while it becomes conditionally stable for $\delta_i>1$ (Chang 2002, 2007a, 2009, 2010, Chen and Ricles 2008, Kolay and Ricles 2014). There is a technique to enlarge the unconditional stability range for a general structure-dependent integration method by using a virtual parameter σ (Chang 2015b). This parameter is named as a stability amplification factor and it can be applied to enlarge the initial stiffness from k_0 to σk_0. As a result, the unconditional stability range is modified from $k_i\le k_0$ to $k_i\le\sigma k_0$ since a structure-dependent integration method has the unconditional stability range of $\delta_i\le 1$. Apparently, the unconditional stability range of a structure-dependent integration method can be effectively enlarged by taking σ to be larger than 1. Hence, it is introduced into the structure-dependent coefficients of the four family methods as shown in Eqs. (3) and (8).

It is important to find the variation of the upper stability limit, which is denoted by $\Omega_0^{(u)}$, with the instantaneous

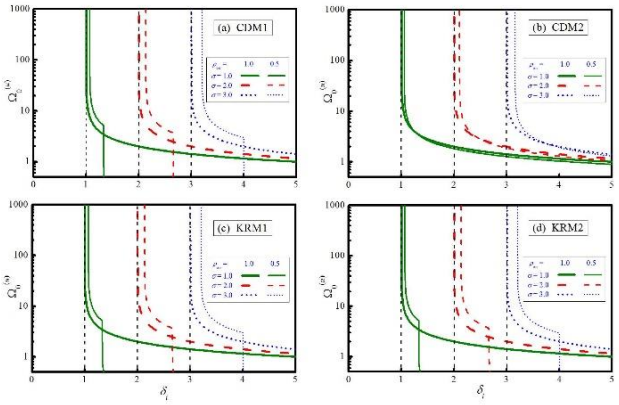

Fig. 6 Variation of upper stability with instantaneous degree of nonlinearity

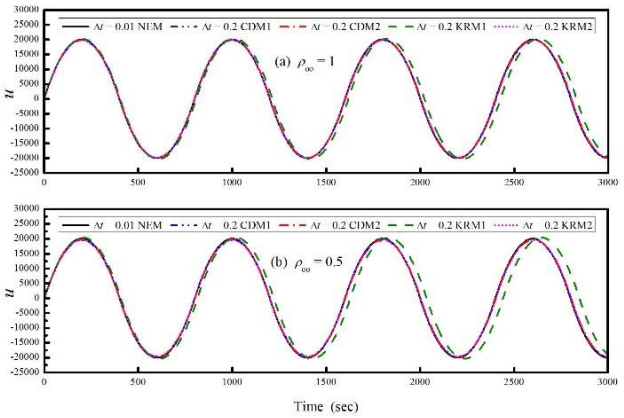

Fig. 7 Free vibration responses to a highly nonlinear system

degree of nonlinearity to confirm the effectiveness of the stability amplification factor. In general, the upper stability limit $\Omega_0^{(u)}$ for each family method for a given value of δ can be numerically calculated. As a result, the calculated results for ρ_∞=1 and 0.5 for all the four family methods are plotted in Fig. 6. In each plot of this figure, it is found that each family method can have an unconditional stability range of $\delta \le \sigma$ for σ=1, 2 and 3 for ρ_∞=1 while it will become conditionally stable in the range of $\delta > \sigma$. Similarly, a slightly larger unconditional stability range can be generally achieved for $\rho_\infty = \frac{1}{2}$ for all the four family methods. Hence, it is verified that the stability amplification factor σ can enlarge the unconditional stability range from $\delta \le 1$ to $\delta \le \sigma$ for a general structure-dependent integration method. On the other hand, for a real structure, its instantaneous stiffness is very rare to become larger than twice of that of the initial stiffness. Hence, $\delta \le 2$ will be generally experienced for practical applications. This implies that the adoption of δ=2 is large enough to have the unconditional stability range of $\delta \le 2$.

In addition to the stability problem for a general nonlinear system, the capability to capture the structural nonlinearity is also closely related to the performance of an integration method in solving a nonlinear system. This capability can be revealed by solving a highly nonlinear system, such as

$$\ddot{u} + \frac{u}{1+|u|} = 0 \tag{11}$$

where u and $\ddot{u}$ denote the displacement and acceleration, respectively. The stiffness 1/(1+|u|) becomes softening after the system deforms. Clearly, a large initial displacement or initial velocity results in a large reduction of the stiffness. The period of the system is $T_0 = 2\pi$ sec determined from the initial stiffness. The displacement responses to the initial conditions of $u(0)=0$ and $\dot{u}(0) = 200$ are calculated and are shown Fig. 7. The result obtained from the Newmark explicit method (NEM) (Newmark 1959) with Δt=0.01sec is treated as a reference solution. Meanwhile, the four family methods with Δt=0.2 sec are also applied to compute the responses. The cases of ρ_∞=1 and 0.5 are taken for each family method. It is seen in Fig. 7 that the results obtained from CDM1, CDM2 and KRM2 are reliable and have the about the same accuracy for both the two cases of ρ_∞=1 and 0.5. However, the numerical results obtained from KRM1 display significant period distortion when compared to the reference solution. These results indicate that CDM1, CDM2 and KRM2 possess almost the same capability to capture structural nonlinearity while KRM1 shows a relatively poor capability for capturing the variation of the nonlinear stiffness when compared to the other three family methods.

It is of interest to explore why KRM1 shows less capability to capture structural nonlinearity than for CDM1, CDM2 and KRM2. In general, a convergence rate can be treated as an indicator of the numerical accuracy of an integration method. Hence, it is natural to identify the convergence rate of each family method. A numerical technique has been employed to identify the convergence rate of displacement, velocity and acceleration for an integration method. In fact, the integration method can be used to solve a problem with a series of small different time steps and then the results can be used to assess the convergence rate of this integration method. In general, the displacement error E_d, velocity error E_v and acceleration error E_a at a given time can be obtained from

$$E_d = \left|d_i - u(t_i)\right|, \quad E_v = \left|v_i - \dot{u}(t_i)\right|, \quad E_a = \left|a_i - \ddot{u}(t_i)\right| \tag{12}$$

where d_i, v_i and a_i are the calculated displacement, velocity and acceleration at the end of the time of t_i while $u(t_i)$, $\dot{u}(t_i)$ and $\ddot{u}(t_i)$ are the exact displacement, velocity and acceleration at the time instant of t_i although they are also obtained from a very small time step. The plot of each error versus step size on a log-log scale can be used to estimate the convergence rate of each error.

For simplicity, the four family methods are used to solve Eq. (11) and the instant time to compute the response errors is chosen to be t=0.1 sec. The variations of E_d, E_v and E_a with Δt are plotted on a log-log scale in Fig. 8. The convergence rate of the specific error for a given family method is equal to the slope of the corresponding curve. All the four family methods can have a convergence rate of 2 for E_d, E_v and E_a for the case of ρ_∞=1 except that for KRM1

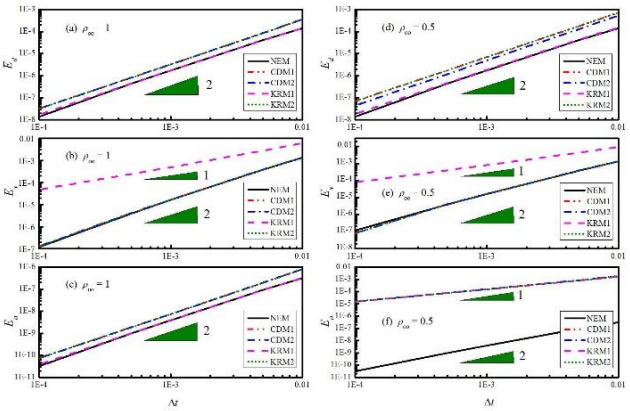

Fig. 8 Convergence rate of displacement, velocity and acceleration

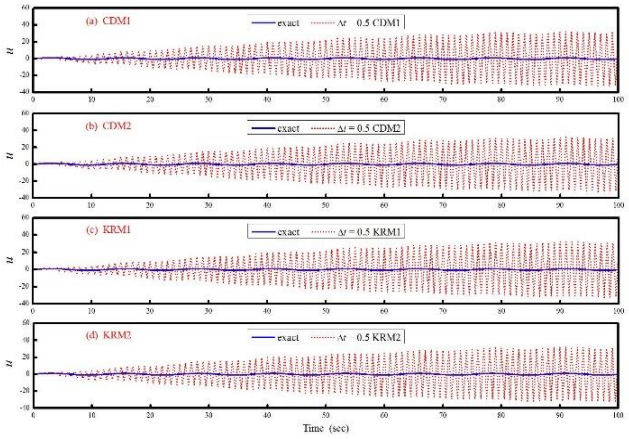

Fig. 9 Forced vibration responses to a sine loading

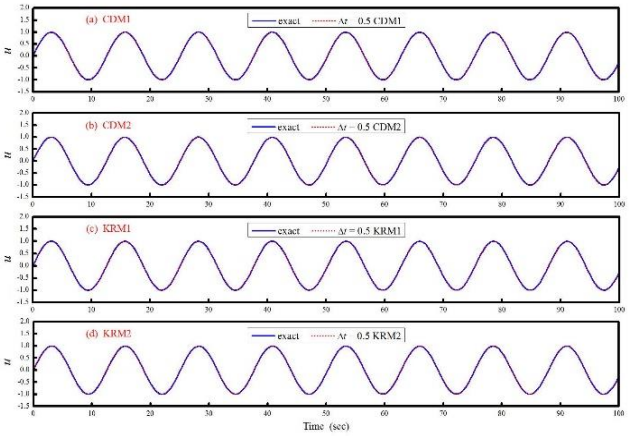

Fig. 10 Forced vibration responses to a sine loading (with a load-dependent term)

only has a convergence rate 1 for E_v. On the other hand, for the case of $\rho_\infty = \frac{1}{2}$, the very similar phenomena are found except that a convergence rate of 1 is found for all the family methods for E_a. Consequently, it seems that KRM1 only has a convergence rate of 1 for E_v for both the cases of ρ_∞=1 and 0.5 is responsible for the poor capability to capture the structural nonlinearity since its convergence rate for E_d and E_a are exactly the same as the other three family methods for both the two cases. Notice that a convergence rate of 1 for E_v for KRM1 might originate from the use of a structure-dependent difference equation for velocity increment since the other three family methods involve the constant coefficients of the difference equation for velocity increment.

5. Unusual overshoot in forced vibration response

Eq. (10) analytically reveals that there is no overshoot in displacement in the free vibration response obtained from the four family methods. However, an unusual overshoot behavior was still experienced in the high frequency forced vibration responses for the four family methods. This type of overshoot is different from that was found by Goudreau and Taylor as shown in Eq. (10) (Chang *et al*. 2016).

In order to illustrate the unusual overshoot in the high frequency forced vibration response, an example is solved by the four family methods.

$$m\ddot{u}(t)+ku(t)=k\sin(\bar{\omega}t) \tag{13}$$

where $\bar{\omega}$ is the applied frequency of the sine loading. The exact solution is found to be

$$u(t)=\frac{1}{1-\omega_r^2}\sin(\bar{\omega}t)-\frac{\omega_r}{1-\omega_r^2}\sin(\omega_0 t) \tag{14}$$

where $\omega_r=\bar{\omega}/\omega_0$ is a frequency ratio. A large ω_r implies a low frequency mode; and then the displacement u is dominated by the transient response. Whereas, a small value of ω_r implies a high frequency mode; and then the displacement u is dominated by the steady-state response. In Eq. (13), the case of m=1, k_0=10^6 and $\bar{\omega}$=1 is considered. The natural frequency of the system is found to be 10^3 rad/sec. The frequency ratio ω_r is 10^{-3} and thus the total response is dominated by the steady-state response. Calculated results obtained from the four family methods with Δt=0.5 sec are shown in Fig. 9.

It is anticipated that a reliable solution can be achieved if the steady-state response is reliably integrated. It has been shown by Chang (2006) that a harmonic load can be accurately represented if a time step corresponding to $\Delta t/\bar{T}\le\frac{1}{12}$ is adopted, where $\bar{T}$ is the period of the applied harmonic load. For this case, the value of $\Delta t/\bar{T}=\frac{1}{4\pi}\le\frac{1}{12}$ implies that the applied sine load can be very accurately captured and thus a reliable steady-state solution can be obtained. However, in Fig. 9, a very significant overshoot is found for all the four family methods. These numerical results are highly inconsistent with the analytical predictions. Hence, the cause of this overshoot must be further investigated.

In order to scrutinize the effect from the dynamic loading to the local truncation error, the local truncation error for each family method is derived from a forced vibration response rather than a free vibration response. As a result, the local truncation errors for the four family methods for zero viscous damping are found to be

$$E=\frac{1}{D_1}\left(\alpha+\gamma-\tfrac{1}{2}\right)\left[\Omega_0\omega_0\dot{u}_i+\tfrac{1}{2}\Omega_0^2\ddot{u}_i-\tfrac{1}{m}\left(f_{i+1}-f_i\right)\right]$$
$$-\frac{1}{D_1}\left(\alpha\gamma-\tfrac{1}{2}\alpha+\beta-\tfrac{1}{12}\right)\left(\Delta t\right)^2\dddot{u}_i$$
$$+\frac{1}{kD_1}\beta\Omega_0^2\ddot{f}_i+O\left[\left(\Delta t\right)^3\right] \qquad \text{CDM1}$$

$$E=-\frac{1}{D_2}\left(\alpha+\gamma-\tfrac{1}{2}\right)\left[\left(\Delta t\right)\ddot{u}_i+\tfrac{1}{2}\left(\Delta t\right)^2\dddot{u}_i\right]$$
$$-\frac{1}{D_2}\left(\beta-\tfrac{1}{12}\right)\left(\Delta t\right)^2\dddot{u}_i+\frac{1}{kD_2}\beta\Omega_0^2\ddot{f}_i \qquad (15)$$
$$+O\left[\left(\Delta t\right)^3\right] \qquad \text{CDM2}$$

$$E=\frac{1}{D_4}\left(\alpha_f-\alpha_m-\gamma+\tfrac{1}{2}\right)\left[\Omega_0\omega_0\dot{u}_i+\tfrac{1}{2}\Omega_0^2\ddot{u}_i-\tfrac{1}{m}\left(f_{i+1}-f_i\right)\right]$$
$$-\frac{1}{D_4}\left(\alpha_f\gamma-\tfrac{1}{2}\alpha_f-\beta+\tfrac{1}{12}\right)\left(\Delta t\right)^2\dddot{u}_i$$
$$-\frac{1}{kD_4}\beta\Omega^2\ddot{f}_i+O\left[\left(\Delta t\right)^3\right] \qquad \text{KRM1, KRM2}$$

where $D_4=2\left[\left(\alpha_m-1\right)+\left(\alpha_f-1\right)2\gamma\xi\Omega_0+\left(\alpha_f-1\right)\beta\Omega_0^2\right]$. It can be found from this equation that the first line of the local truncation error for CDM1 and CDM2 will become zero since $\gamma=\frac{1}{2}-\alpha$ is often adopted to have desired numerical properties as shown in Eq. (4). Hence, the local truncation error of CDM1 will be dominated by the term $\beta\Omega_0^2\ddot{f}_i/\left(kD_1\right)$ for a high frequency mode since this term is quadratically proportional to Ω_0. Similarly, the local truncation error of CDM2 is dominated by the term $\beta\Omega_0^2\ddot{f}_i/\left(kD_2\right)$ for a high frequency mode. On the other hand, the first line of the local truncation error for KRM1 and KRM2 will disappear since $\gamma=\frac{1}{2}-\alpha_m+\alpha_f$ is often taken in Eq. (9) so that the desired numerical properties can be achieved. As a result, the dominant error terms of KRM1 and KRM2 are found to be $\beta\Omega_0^2\ddot{f}_i/\left(kD_4\right)$ for high frequency modes. It is worth noting that the dominant error terms of the four family methods are quadratically proportional to Ω_0. Thus, it is implied that the unusual overshoot will be significant for a high frequency mode while it might be insignificant for a low frequency mode.

After figuring out the root cause of this type of overshoot, it is very important to propose a remedy to eliminate the unusual overshoot. For this purpose, a load-dependent term is introduced into the difference equation for displacement increment to eliminate the adverse dominant error term. As a result, the load-dependent term for each family method is found to be

$$p_{i+1}=\frac{1}{D_1}\beta\sigma\tfrac{1}{m}\left(\Delta t\right)^2\left(f_{i+1}-f_i\right)$$
$$+\frac{1}{D_1}\alpha\beta\sigma\tfrac{1}{m}\left(\Delta t\right)^2\left(f_{i+1}-2f_i+f_{i-1}\right) \qquad \text{CDM1}$$

$$p_{i+1}=\frac{1}{D_2}\beta\sigma\tfrac{1}{m}\left(\Delta t\right)^2\left(f_{i+1}-f_i\right) \qquad \text{CDM2}$$
$$p_{i+1}=\frac{1}{D_4}\beta\sigma\tfrac{1}{m}\left(\Delta t\right)^2\left(f_{i+1}-f_i\right) \qquad \text{KRM1, KRM2} \qquad (16)$$

After introducing the load-dependent term p_{i+1} into the difference equation for displacement increment for each family method, the dominant error term for each family method can be automatically eliminated. Hence, the unusual overshoot behavior in the high frequency forced vibration responses can be removed for each family method. In order to confirm the effectiveness of this load-dependent term, Eq. (13) is solved again by using the four family methods and the results are plotted in Fig. 10. Apparently, the results obtained from the four family methods are almost coincided together with the exact solution. Consequently, it seems that the load-dependent term must be included in the original formulation of a structure-dependent integration method so that there will be no overshoot phenomenon in the high frequency forced vibration responses.

6. Unusual weak instability property

In Fig. 4(c), a very significant overshooting behavior was experienced for KRM1 with ρ_∞=1. This phenomenon is totally contradictory to the analytical prediction as shown in Eq. (10) for KRM1. Whereas, no overshoot was found for CDM1, CDM2 and KRM2 as shown in Figs. 4(a), 4(b) and 4(d); and these results are consistent with the analytical predictions as shown in Eq. (10) for CDM1, CDM2 and KRM2. Hence, the unusual overshoot in Fig. 4(c) for KRM1 must be further investigated. In fact, it will be numerically illustrated first and subsequently analytically verified that an unusual overshoot will experience for KRM1 and KRM2 in the high frequency responses to nonzero initial conditions while there is no such an unusual overshoot property for CDM1 and CDM2.

A linear elastic 2-degree of freedom system is designed to illustrate such an unusual overshoot behavior. As a result, the following equations of motion are considered

$$\begin{bmatrix}1&0\\0&1\end{bmatrix}\begin{Bmatrix}\ddot{u}_1\\\ddot{u}_2\end{Bmatrix}+\begin{bmatrix}5\times10^n+2\times10^2&-5\times10^n\\-5\times10^n&5\times10^n\end{bmatrix}\begin{Bmatrix}u_1\\u_2\end{Bmatrix}=\begin{Bmatrix}0\\0\end{Bmatrix} \qquad (17)$$

The cases of n=1, 5 and 9 are adopted to simulate the three systems S1, S2 and S3, respectively. The natural frequencies of S1 are found to be ω_1=6.18 and ω_2=16.18 rad/sec; and the modal shapes are

$$\phi_1=\begin{Bmatrix}0.236\\1.000\end{Bmatrix} \quad , \quad \phi_2=\begin{Bmatrix}-4.236\\1.000\end{Bmatrix} \qquad (18)$$

Similarly, the natural frequencies for S2 are found to be ω_1=10 and ω_2=10^3 rad/sec while those are ω_1=10 and ω_2=10^5 for S3. The modal shapes for S2 and S3 are almost the same and are

$$\phi_1=\begin{Bmatrix}1\\1\end{Bmatrix}, \quad \phi_2=\begin{Bmatrix}1\\-1\end{Bmatrix} \qquad (19)$$

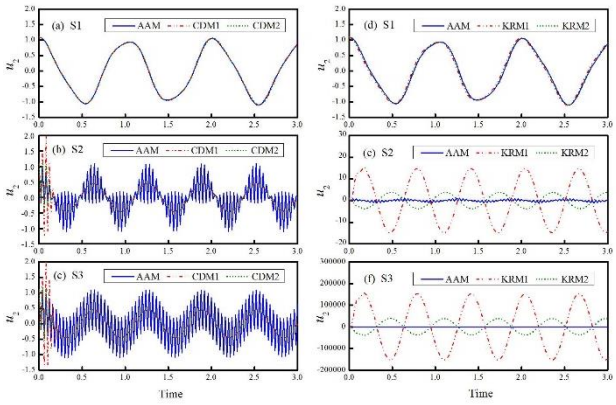

Fig. 11 Free vibration responses to three 2-DOF linear elastic systems

The following initial conditions will be examined for S1, S2 and S3.

$$\mathbf{u}_0 = \begin{Bmatrix} u_1(0) \\ u_2(0) \end{Bmatrix} = \phi_1 + \frac{1}{10}\phi_2 = \begin{Bmatrix} -0.19 \\ 1.10 \end{Bmatrix} \quad \text{S1}$$
$$\mathbf{u}_0 = \begin{Bmatrix} u_1(0) \\ u_2(0) \end{Bmatrix} = \phi_1 + \frac{1}{10}\phi_2 = \begin{Bmatrix} 1.1 \\ 0.9 \end{Bmatrix} \quad \text{S2, S3} \tag{20}$$

where $\mathbf{u}_0$ is made up of one time of the first modal shape and one-tenth of the second modal shape.

The four family methods with $\rho_\infty = \frac{1}{2}$ are applied to calculate the free vibration responses for S1, S2 and S3 by Δt=0.02 sec. In addition, the constant average acceleration method (AAM) with Δt=0.02 sec is also used to yield the free vibration responses to $\mathbf{u}_0$ with a zero initial velocity vector and the solution is considered as a reference solution for comparison. As a result, numerical solutions of u_2 for the three systems are plotted in Fig. 11. It is manifested from Figs. 11(a) and 11(d) that all the four family methods can provide accurate solutions for S1 with two relatively low frequency modes. However, very different phenomena are found for the numerical results of S2 and S3 for using different family methods. It is worth noting that the high frequency second mode of S2 and S3 cannot be accurately integrated for using the time step of $\Delta t = 0.02$ sec for all the four family methods and AAM. Hence, the result obtained from AAM includes an accurate response of the first mode and an inaccurate response of the second mode, where the amplitude of the second mode is preserved although period is significantly distorted for both S2 and S3. In Figs. 11(b) and 11(c), either CDM1 or CDM2 can suppress or even eliminate the high frequency second mode very rapidly and thus no overshoot is found in the free vibration responses. Whereas, a significant overshoot is found in the responses obtained from KRM1 and KRM2 for both S2 and S3 as shown in Figs. 11(e) and 11(f). It is also found that the overshoot phenomenon in the response of KRM1 is much more significant than for KRM2 for both S2 and S3.

In order to figure out the root cause of the unusual overshoot for KRM1 and KRM2 as well as no overshoot for both CDM1 and CDM2, an analytical scheme will be applied to derive the numerical solution, which is obtained from each family method, in a mathematical form. For this purpose, the free vibration response of an undamped, linear elastic single degree of freedom system will be solved by using the four family methods. Hence, the equation of motion can also be expressed as shown in Eq. (13) except that a zero dynamic loading is considered. The initial conditions are taken to be the initial displacement of d_0 and initial velocity of v_0. For comparison purpose, the free vibration response to these initial conditions of an undamped, linear elastic single degree of freedom system can be obtained from the fundamental theory of structural dynamics. As a result, the theoretical solution is found to be

$$d_n = \cos\left(n\Omega_0\right)d_0 + \frac{\sin\left(n\Omega_0\right)}{\Omega_0}\left(\Delta t\right)v_0 \tag{21}$$

where d_n=u(t_n) and t_n=n(Δt).

Meanwhile, the step-by-step integration procedure of applying each family method to solve the same problem can be written as a recursive matrix form and is

$$\mathbf{X}_n = \mathbf{A}\mathbf{X}_{n-1} = \mathbf{A}^2\mathbf{X}_{n-2} = \cdots\cdots = \mathbf{A}^n\mathbf{X}_0 \tag{22}$$

where $\mathbf{X}_n = \left[d_n,\ (\Delta t)v_n,\ (\Delta t)^2 a_n\right]^{\mathrm{T}}$ and $\mathbf{X}_0 = \left[d_0,\ (\Delta t)v_0,\ (\Delta t)^2 a_0\right]^{\mathrm{T}}$. Hence, for the given initial conditions of d_0 and v_0, the initial acceleration a_0 can be determined from the equation of motion and is found to be $(\Delta t)^2 a_0 = -2\xi\Omega_0(\Delta t)v_0 - \Omega_0^2 d_0$ for the free vibration response. In general, if there exist three linearly independent eigenvectors, Eq. (22) can further reduce to be

$$\mathbf{X}_n = \mathbf{A}^n\mathbf{X}_0 = \mathbf{\Phi}\mathbf{\Lambda}^n\mathbf{\Phi}^{-1}\mathbf{X}_0 \tag{23}$$

where

$$\mathbf{\Lambda} = \begin{bmatrix} \lambda_1 & 0 & 0 \\ 0 & \lambda_2 & 0 \\ 0 & 0 & \lambda_3 \end{bmatrix},\quad \mathbf{\Phi} = \begin{bmatrix} \phi_1 & \phi_2 & \phi_3 \end{bmatrix} \tag{24}$$

where $\mathbf{\Lambda}$ is a diagonal matrix and its diagonal term λ_i, i=1,2,3, is an eigenvalue of the matrix $\mathbf{A}$; $\mathbf{\Phi}$ is an eigenvector matrix and each column ϕ_i, i=1,2,3, is the eigenvector corresponding to λ_i. On the other hand, an amplification matrix $\mathbf{A}$ might not be diagonalized for an integration method if it is lack of three linearly independent eigenvectors. In this case, Eq. (23) is not applicable. However, there will exist a non-singular matrix $\mathbf{\Psi}$ to transform the matrix $\mathbf{A}$ into a Jordan canonical form such as $\mathbf{A}=\mathbf{\Psi}\mathbf{J}\mathbf{\Psi}^{-1}$, where $\mathbf{J}$ is the Jordan form of the matrix $\mathbf{A}$. As a result, Eq. (22) can be rewritten as

$$\mathbf{X}_n = \mathbf{A}^n\mathbf{X}_0 = \mathbf{\Psi}\mathbf{J}^n\mathbf{\Psi}^{-1}\mathbf{X}_0 \tag{25}$$

Hence, the following equation can be achieved

$$\mathbf{J} = \begin{bmatrix} \lambda & 1 & 0 \\ 0 & \lambda & 1 \\ 0 & 0 & \lambda \end{bmatrix},\quad \mathbf{\Psi} = \begin{bmatrix} \psi_1 & \psi_2 & \psi_3 \end{bmatrix} \tag{26}$$

if the amplification matrix $\mathbf{A}$ has a triple root and there is

only a linearly independent eigenvector. As a result, either Eq. (23) or (25) can be applied to analytically derive the numerical solution in a mathematical form.

Since the overshoot behaviors were found in the high frequency responses to nonzero initial conditions for KRM1 and KRM2, it is of interest to obtain the numerical solution in a mathematical form for each family method in the limit $\Omega_0\to\infty$. It is very complex to analytically obtain the three linearly independent eigenvectors for a general value of α for either CDM1 or CDM2 and then to apply Eq. (23) to derive the numerical solution in a mathematical form. For simplicity, the special case of α=0 is considered for CDM1 and CDM2. Notice that they will become exactly the same integration method for α=0. In addition, the three eigenvalues of this integration method are found to be $\lambda_{1,2}=-1$ and $\lambda_3=0$ in the limit $\Omega_0\to\infty$. In addition, the corresponding eigenvector matrix is found to be

$$\mathbf{\Phi}=\begin{bmatrix} 1 & 1 & \frac{\frac{1}{4}}{1+\frac{1}{4}\Omega_0^2} \\ j\Omega_0 & -j\Omega_0 & \frac{-\frac{1}{2}}{1+\frac{1}{4}\Omega_0^2} \\ -\Omega_0^2 & -\Omega_0^2 & \frac{1}{1+\frac{1}{4}\Omega_0^2} \end{bmatrix} \tag{27}$$

Since these three eigenvectors are linearly independent and thus the amplification matrix **A** of CDM1 or CDM2 for α=0 is diagonalizable. Consequently, using Eq. (23), it is very straightforward to obtain the numerical solution in a mathematical form for d_n and it can be simply expressed as

$$d_n=\cos\left(n\bar{\Omega}_0\right)d_0+\frac{\sin\left(n\bar{\Omega}_0\right)}{\Omega_0}\left(\Delta t\right)v_0 \tag{28}$$

where $\bar{\Omega}_0=\cos^{-1}\left[\left(1-\frac{1}{4}\Omega_0^2\right)/\left(1+\frac{1}{4}\Omega_0^2\right)\right]$.

Similarly, it is found that both KRM1and KRM2 have the same the characteristic equation in the limit $\Omega_0\to\infty$. In addition, a triple real root is found for the characteristic equation and it is

$$\lambda_1=\lambda_2=\lambda_3=-\rho_\infty \tag{29}$$

For this case, there is only one linearly independent eigenvector for either KRM1 or KRM2 and is found to be

$$\psi_1=\begin{Bmatrix} 1 \\ 1+\rho_\infty \\ -\Omega_0^2 \end{Bmatrix} \quad \text{KRM1}$$
$$\psi_1=\begin{Bmatrix} 1 \\ \left(\frac{1}{2}-\frac{1}{1+\rho_\infty}\right)\Omega_0^2 \\ -\Omega_0^2 \end{Bmatrix} \quad \text{KRM2} \tag{30}$$

Both KRM1 and KRM2 have no three linearly independent eigenvectors. Hence, their amplification matrices cannot be diagonalized. However, a non-singular matrix $\mathbf{\Psi}$ can be found to transform the matrix **A** into a Jordan canonical form as shown in Eq. (25). As a result, the non-singular matrix for KRM1 is found to be

$$\mathbf{\Psi}_1=\begin{bmatrix} 1 & 1 & 1 \\ 1+\rho_\infty & 2+\rho_\infty & 2+\rho_\infty+\frac{2}{1+\rho_\infty} \\ -\Omega_0^2 & -\Omega_0^2 & -\left[1+\frac{1}{(1+\rho_\infty)^2}\right]\Omega_0^2 \end{bmatrix} \tag{31}$$

while that for KRM2 is

$$\mathbf{\Psi}_2=\begin{bmatrix} 1 & 1 & 1 \\ \left(\frac{1}{2}-\frac{1}{1+\rho_\infty}\right)\Omega_0^2 & \left[\frac{1}{2}-\frac{\rho_\infty}{(1+\rho_\infty)^2}\right]\Omega_0^2 & \left[\frac{1}{2}+\frac{\frac{1}{2}-\rho_\infty}{(1+\rho_\infty)^2}\right]\Omega_0^2 \\ -\Omega_0^2 & -\Omega_0^2 & -\left[1+\frac{1}{(1+\rho_\infty)^2}\right]\Omega_0^2 \end{bmatrix} \tag{32}$$

Meanwhile, the term $\mathbf{J}^n$ in Eq. (25) can be obtained after a simple calculation and the result is found to be

$$\mathbf{J}^n=\begin{bmatrix} \lambda^n & n\lambda^{n-1} & n(n-1)\lambda^{n-2} \\ 0 & \lambda^n & n\lambda^{n-1} \\ 0 & 0 & \lambda^n \end{bmatrix}, \quad n>1 \tag{33}$$

where the upper off-diagonal terms of the matrix $\mathbf{J}^n$ are nonzero.

After substituting Eqs. (31) to (33) into Eq. (25), the numerical solutions of d_n in mathematical forms for KRM1 and KRM2 are found to be

$$\begin{aligned} d_n&=-\left[(n+1)\rho_\infty+n\right](-\rho_\infty)^{n-1}d_0 \\ &\quad +n(-\rho_\infty)^{n-1}(\Delta t)v_0 \qquad \text{KRM1} \\ d_n&=\left[\tfrac{1}{2}n-\rho_\infty-\tfrac{1}{2}n(\rho_\infty)^2\right](-\rho_\infty)^{n-1}d_0 \\ &\quad +\frac{(1+\rho_\infty)^2}{\Omega_0^2}n(-\rho_\infty)^{n-1}(\Delta t)v_0 \qquad \text{KRM2} \end{aligned} \tag{34}$$

Either the first line or the second line of this equation reveals that the numerical solution obtained from KRM1 or KRM2 is entirely different from the theoretical solution as shown in Eq. (21) since the basic forms of the numerical solutions are drastically different from those of the theoretical solutions. It is of great interest to consider the special case of ρ_∞=1 for both KRM1 and KRM2. As a result, Eq. (34) becomes

$$\begin{aligned} d_n&=(2n+1)(-1)^n d_0+n(-1)^{n-1}(\Delta t)v_0 \qquad \text{KRM1} \\ d_n&=(-1)^n d_0+\frac{4n(-1)^{n-1}}{\Omega_0^2}(\Delta t)v_0 \qquad \text{KRM2} \end{aligned} \tag{35}$$

For comparisons, the coefficients of d_0 and $(\Delta t)v_0$ are summarized in Table 1 for α=0 for CDM1 and CDM2 as well as ρ_∞=1 for KRM1 and KRM2. Both the third and fourth rows of Table 1 reveal that the coefficients of d_0 and $(\Delta t)v_0$ for CDM1 and CDM2 with α=0 are almost the same as those of the theoretical solution except for the period distortion from Ω_0 to $\bar{\Omega}_0$. Thus, there will be no overshoot for CDM1 and CDM2 with α=0 since both the sine and cosine terms are bounded in the range of −1 and 1.

Table 1 Comparisons of coefficients for d_0 and $(\Delta t)v_0$

Method	Coefficient of d_0	Coefficient of $(\Delta t)v_0$
Exact	$\cos(n\Omega_0)$	$\sin(n\Omega_0)/\Omega_0$
CDM1 (α=0)	$\cos(n\bar{\Omega}_0)$	$\sin(n\bar{\Omega}_0)/\Omega_0$
CDM2 (α=0)	$\cos(n\bar{\Omega}_0)$	$\sin(n\bar{\Omega}_0)/\Omega_0$
KRM1 (ρ_∞=1)	$(2n+1)(-1)^n$	$n(-1)^{n+1}$
KRM2 (ρ_∞=1)	$(-1)^n$	$4n(-1)^{n-1}/\Omega_0^2$

On the other hand, for the general case of $-\frac{1}{3} \le \alpha < 0$ for CDM1, the three eigenvalues are $\lambda_{1,2}=-\rho_\infty$ and $\lambda_3=\rho_\infty-1$ in the limit $\Omega_0\to\infty$ while for the case of $-1\le\alpha<0$ for CDM2, the eigenvalues are found to be $\lambda_{1,2}=-\rho_\infty$ and $\lambda_3=0$. In addition, it is numerically verified that either CDM1 or CDM2 has three linearly independent eigenvectors and thus their amplification matrices are diagonalizable. Hence, they have no unusual overshoot.

It is manifested from the fifth row that the coefficients of d_0 and $(\Delta t)v_0$ for KRM1 with ρ_∞=1 increases with the increase of time step and are drastically different those the theoretical solution. Hence, a significant overshoot behavior is expected. Similar results are also found in the first line of Eq. (34) for KRM1 with $0\le\rho_\infty<1$ except that overshoot behaviors will be reduced due to $0\le\rho_\infty<1$. On the other hand, the last column shows that the coefficient of d_0 for KRM2 with ρ_∞=1 will jump from −1 to 1 alternatively while that of $(\Delta t)v_0$ will increase with the increase of the number of time step for a given Ω_0. Consequently, an overshoot behavior is also expected. However, the overshoot phenomenon for KRM2 will be less significant than for KRM1 due to smaller coefficients. Again, the behavior for KRM2 with $0\le\rho_\infty<1$ will be similar to that of KRM2 with ρ_∞=1 except that the overshoot phenomenon will become less significant due to $0\le\rho_\infty<1$. This is confirmed by Figs. 11(e) and 11(f).

These analytical results may be applied to explain the phenomena found in Fig. 4. In Fig. 4, the period of the system is taken as 0.1sec and a step size Δt=1 sec is adopted for time integration. Thus, $\omega_0=20\pi$ rad/sec and $\Omega_0=20\pi$, which is not very large when compared to $\Omega_0\to\infty$. Since the value of $\Omega_0=20\pi$ is not very large, no overshoot was generally found in Figs. 4(c) and 4(d) for KRM1 and KRM2 except that for KRM1 with ρ_∞=1 the solution shows an overshoot behavior. This might be manifested from the first line of Eq. (35), where both the absolute coefficients of d_0 and $(\Delta t)v_0$ are much larger than those of the theoretical solution. In fact, they are found to be $(2n+1)$ and n for d_0 and $(\Delta t)v_0$, respectively, for KRM1. Whereas, they are found to be $|\cos(n\Omega_0)| \le 1$ and $|\sin(n\Omega_0)/\Omega_0| \le 1/(20\pi)$ in theoretical solution correspondingly.

Since the growth of the numerical solution d_n is linear in n for both KRM1 and KRM2 as ρ_∞=1, thus a weak instability will experience for both the two family methods as ρ_∞=1. In general, a weak instability is referred to the polynomial growth in n of arbitrary order (Belytschko and Hughes 1983). Notice that the growth of the weak instability is considerably weaker than that of the instability caused by the spectral radius larger than 1. As a summary, either KRM1 or KRM2 has an adverse weak instability property as ρ_∞=1 for nonzero initial conditions due to the lack of three linearly independent eigenvectors for high frequency modes. Hence, they are hardly acceptable for practical applications (Penzien 2004, Su and Xu 2014). On the other hand, CDM1 and CDM2 have no such an adverse weak instability property since they can have three linearly independent eigenvectors and thus their performances are much better than for KRM1 and KRM2 based on stability consideration.

Table 2 Comparison of numerical properties

Property	CDM1	CDM2	KRM1	KRM2
Unconditional stability	Yes	Yes	Yes	Yes
Second-order accuracy	Yes	Yes	Yes	Yes
Explicit formulation	Yes	Yes	Yes	Yes
Controllable numerical damping	Yes	Yes	Yes	Yes
Overshoot (old type)	No	No	No	No
Overshoot (new type)	No	No	No	No
Weak instability	No	No	Yes	Yes
Nonlinear performance	Good	Good	Poor	Good

Overshoot (old type = independent of dynamic loading; found by Goudreau and Taylor)
Overshoot (new type = dependent upon dynamic loading; removed by adding a load-dependent term)

7. Conclusions

For brevity, Table 2 summarizes the major numerical properties of the four family methods. It is found that the numerical properties of period distortion, numerical damping ratio and spectral radius for linear elastic systems are exactly the same for the four family methods of CDM1, KRM1 and KRM2. Whereas, CDM2 generally shows more numerical damping ratio, more period distortion and thus less spectral radius when compared to the other three family methods. It is confirmed by the four family methods that a structure-dependent integration method generally has unconditional stability for linear elastic and stiffness softening systems, i.e., $\delta_i\le1$, while it is conditionally stable for stiffness hardening systems, i.e. $\delta_i>1$. A stability amplification factor σ can be applied to enlarge the unconditional stability range from $\delta_i\le1$ to $\delta_i\le\sigma$. Since it is very rare to experience that the instantaneous stiffness of a real structure will become larger than twice of the initial stiffness, the choice of σ=2 seems large enough for general applications. Although an unusual overshoot in the high frequency forced vibration response will generally experience for the four family methods, the introduction of a load-dependent term into the difference equation for displacement increment for each family method can effectively eliminate the adverse overshooting behavior.

The most detrimental property to KRM1 and KRM2 is a weak instability or overshoot in the high frequency responses to nonzero initial conditions. Thus, the numerical solutions obtained from either KRM1 or KRM2 may experience an overshoot or even numerical instability for

nonzero initial conditions. This is a very severe limitation and therefore its applications might be of no interest. The cause of this weak instability is due to the lack of three linearly independent eigenvectors for the high frequency modes and thus the amplification matrix cannot be diagonalized. On the other hand, CDM1 and CDM2 can have three linearly independent eigenvectors for the high frequency modes and thus their amplification matrices are diagonalizable and they have no such an adverse weak instability property or overshooting. Although KRM1 and KRM2 can generally have the same properties as those of CDM1 and CDM2, the weak instability or overshoot for nonzero initial conditions will stringently prevent them from practical applications. Thus, CDM1 and CDM2 are preferable over KRM1 and KRM2 although they are classified as the two-step integration methods. Since CDM1 and CDM2 can integrate unconditional stability, explicit formulation and controllable numerical dissipation simultaneously, they can be competitive with the traditional implicit dissipative methods, such as the HHT-α method, WBZ-α method and the generalized-α method due to no involvement of nonlinear iterations for each time step.

Acknowledgments

The author is grateful to acknowledge that this study is financially supported by the National Science Council, Taiwan, R.O.C., under Grant No.NSC-105-2221-E-027-029.

References

Alamatian, J. (2013), "New implicit higher order time integration for dynamic analysis", *Struct. Eng. Mech.*, **48**(5), 711-736.

Bathe, K.J. and Noh, G. (2012), "Insight into an implicit time integration scheme for structural dynamics", *Comput. Struct.*, **98-99**, 1-6.

Bathe, K.J. and Wilson, E.L. (1973), "Stability and accuracy analysis of direct integration methods", *Earthq. Eng. Struct. Dyn.*, **1**, 283-291.

Belytschko, T. and Hughes, T.J.R. (1983), *Computational Methods for Transient Analysis*, Elsevier Science Publishers B.V., North-Holland, Amsterdam.

Chang, S.Y. (2002), "Explicit pseudodynamic algorithm with unconditional stability", *J. Eng. Mech.*, ASCE, **128**(9), 935-947.

Chang, S.Y. (2006), "Accurate representation of external force in time history analysis", *J. Eng. Mech.*, ASCE, **132**(1), 34-45.

Chang, S.Y. (2007a), "Enhanced unconditionally stable explicit pseudodynamic algorithm", *J. Eng. Mech.*, ASCE, **133**(5), 541-554.

Chang, S.Y. (2007b), "Improved explicit method for structural dynamics", *J. Eng. Mech.*, ASCE, **133**(7), 748-760.

Chang, S.Y. (2009), "An explicit method with improved stability property", *Int. J. Numer. Meth. Eng.*, **77**(8), 1100-1120.

Chang, S.Y. (2010), "A new family of explicit method for linear structural dynamics", *Comput. Struct.*, **88**(11-12), 755-772.

Chang, S.Y. (2014a), "Family of structure-dependent explicit methods for structural dynamics", *J. Eng. Mech.*, ASCE, **140**(6), 06014005.

Chang, S.Y. (2014b), "Numerical dissipation for explicit, unconditionally stable time integration methods", *Earthq. Struct.*, **7**(2), 157-176.

Chang, S.Y. (2014c), "A family of non-iterative integration methods with desired numerical dissipation", *Int. J. Numer. Meth. Eng.*, **100**(1), 62-86.

Chang, S.Y. (2015a), "Dissipative, non-iterative integration algorithms with unconditional stability for mildly nonlinear structural dynamics", *Nonlin. Dyn.*, **79**(2), 1625-1649.

Chang, S.Y. (2015b), "A general technique to improve stability property for a structure-dependent integration method", *Int. J. Numer. Meth. Eng.*, **101**(9), 653-669.

Chang, S.Y., Wu, T.H. and Tran, N.C. (2015), "A family of dissipative structure-dependent integration methods", *Struct. Eng. Mech.*, **55**(4), 815-837.

Chang, S.Y., Wu, T.H. and Tran, N.C. (2016), "Improved formulation for a structure-dependent integration method", *Struct. Eng. Mech.*, **60**(1), 149-162.

Chen, C. and Ricles, J.M. (2008), "Development of direct integration algorithms for structural dynamics using discrete control theory", *J. Eng. Mech.*, ASCE, **134**(8), 676-683.

Chung, J. and Hulbert, G.M. (1993), "A time integration algorithm for structural dynamics with improved numerical dissipation: the generalized- method", *J. Appl. Mech.*, **60**(6), 371-375.

Civalek, O. (2006), "Harmonic differential quadrature-finite differences coupled approaches for geometrically nonlinear static and dynamic analysis of rectangular plates on elastic foundation", *J. Sound Vib.*, **294**(4), 966-980.

Civalek, O. (2007), "Nonlinear dynamic response of MDOF systems by the method of harmonic differential quadrature (HDQ)", *Struct. Eng. Mech.*, **25**(2), 201-217.

Civalek, O. (2013), "Nonlinear dynamic response of laminated plates resting on nonlinear elastic foundations by the discrete singular convolution-differential quadrature coupled approaches", *Compos. Part B: Eng.*, **50**, 171-179.

Fung, T.C. (2001), "Solving initial value problems by differential quadrature method-Part 2: second-and higher-order equations", *Int. J. Numer. Meth. Eng.*, **50**, 1429-1454.

Fung, T.C. (2002), "Stability and accuracy of differential quadrature method in solving dynamic problems", *Comput. Meth. Appl. Mech. Eng.*, **191**, 1311-1331.

Gao, Q., Wu, F., Zhang, H.W., Zhong, W.X., Howson, W.P. and Williams, F.W. (2012), "A fast precise integration method for structural dynamics problems", *Struct. Eng. Mech.*, **43**(1), 1-13.

Goudreau, G.L. and Taylor, R.L. (1972), "Evaluation of numerical integration methods in elasto-dynamics", Computer Methods in Applied Mechanics and Engineering, **2**, 69-97.

Gui, Y., Wang, J.T., Jin, F., Chen, C. and Zhou, M.X. (2014), "Development of a family of explicit algorithms for structural dynamics with unconditional stability", *Nonlin. Dyn.*, **77**(4), 1157-1170.

Hadianfard, M.A. (2012), "Using integrated displacement method to time-history analysis of steel frames with nonlinear flexible connections", *Struct. Eng. Mech.*, **41**(5), 675-689.

Hilber, H.M. and Hughes, T.J.R. (1978), "Collocation, dissipation, and 'overshoot' for time integration schemes in structural dynamics", *Earthq. Eng. Struct. Dyn.*, **6**, 99-118.

Hilber, H.M., Hughes, T.J.R. and Taylor, R.L. (1977), "Improved numerical dissipation for time integration algorithms in structural dynamics", *Earthq. Eng. Struct. Dyn.*, **5**, 283-292.

Kolay, C. and Ricles, J. (2016), "Assessment of explicit and semi-explicit classes of model-based algorithms for direct integration in structural dynamics", *Int. J. Numer. Meth. Eng.*, **107**, 49-73.

Kolay, C. and Ricles, J.M. (2014), "Development of a family of unconditionally stable explicit direct integration algorithms with controllable numerical energy dissipation", *Earthq. Eng. Struct. Dyn.*, **43**, 1361-1380.

Krenk, S. (2008), "Extended state-space time integration with high-frequency energy dissipation", *Int. J. Numer. Meth. Eng.*,

73, 1767-1787.
Newmark, N.M. (1959), "A method of computation for structural dynamics", *J. Eng. Mech. Div.*, ASCE, **85**, 67-94.
Penzien, J. (2004), "Dynamic analysis of structure/foundation systems", *Struct. Eng. Mech.*, **17**(3), 281-290.
Su, C. and Xu, R. (2014), "Random vibration analysis of structures by a time-domain explicit formulation method", *Struct. Eng. Mech.*, **52**(2), 239-260.
Wood, W.L., Bossak, M. and Zienkiewicz, O.C. (1981), "An alpha modification of Newmark's method", *Int. J. Numer. Meth. Eng.*, **15**, 1562- 1566.

PL